Journal of Hazardous Materials 429 (2022) 128274

Contents lists available at ScienceDirect

Journal of Hazardous Materials

journal homepage: www.elsevier.com/locate/jhazmat

Research Paper

Effects of Fe(II)-induced transformation of scorodite on arsenic solubility

Jimei Zhou [a,b,1], Yizhang Liu [a,1], Hongling Bu [c], Peng Liu [d], Jing Sun [a], Fei Wu [a,b,c], Jian Hua [a,e], Chengshuai Liu [a,c,*]

[a] State Key Laboratory of Environmental Geochemistry, Institute of Geochemistry, Chinese Academy of Sciences, Guiyang 550081, PR China
[b] University of Chinese Academy of Sciences, Beijing 100049, PR China
[c] National-Regional Joint Engineering Research Center for Soil Pollution Control and Remediation in South China, Guangdong Key Laboratory of Integrated Agro-environmental Pollution Control and Management, Institute of Eco-environmental and Soil Sciences, Guangdong Academy of Sciences, Guangzhou 510650, PR China
[d] School of Environmental Studies & State Key Laboratory of Biogeology and Environmental Geology, China University of Geosciences, Wuhan 430074, PR China
[e] School of Resources and Environmental Science, Wuhan University, Wuhan 430079, PR China

HIGHLIGHTS

- Fe(II)-induced transformation of scorodite increased As solubility.
- A considerable fraction of structural As transformed to extractable phase.
- The amount of As released from scorodite was the greatest with 1 mM Fe(II).
- Reduction of As(V) to As(III) occurred during scorodite transformation.
- Parasymplesite and ferrihydrite-like were important for As immobilization.

GRAPHICAL ABSTRACT

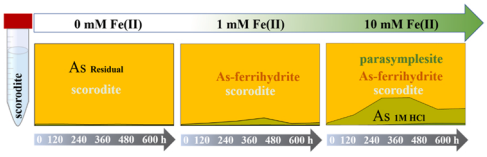

ARTICLE INFO

Editor: Dr. L. Haizhou

Keywords:
Scorodite
Fe(II)-induced transformation
Parasymplesite
Ferrihydrite-like
Arsenic repartition

ABSTRACT

Scorodite ($FeAsO_4{\cdot}2H_2O$) is a pivotal secondary ferric arsenate that immobilizes most of arsenic (As) in acidic As-contaminated environments, but secondary As pollution may occur during dissolution of scorodite in environments involving redox changes. Reductive dissolution of scorodite by coexisting dissolved Fe^{2+} ($Fe(II)_{aq}$) under anaerobic conditions and its effects on the behavior of As have yet to be examined. Here, this study monitored the changes in mineralogy, solubility and speciation of As during scorodite transformation induced by Fe(II) under anaerobic conditions at pH 7.0 and discussed the underlying mechanisms. Mössbauer and X-ray diffraction (XRD) analysis showed the formation of parasymplesite and ferrihydrite-like species during scorodite transformation, which was highly controlled by $Fe(II)_{aq}$ concentrations. 1 mM $Fe(II)_{aq}$ enhanced As mobilization into the solution, whereas As was repartitioned to the PO_4^{3-}-extractable and HCl-extractable phases with 5 and 10 mM Fe(II). The neo-formed parasymplesite and ferrihydrite-like species immobilized dissolved As(V) through adsorption and incorporation. Additionally, As(V) reduction occurred during Fe(II)-induced scorodite transformation. Our results provide new insights into the stability and risk of scorodite in anaerobic environments as well as the geochemical behavior of As in response to Fe cycling.

* Correspondence to: No. 99 Lincheng Road West, Guanshanhu District, Guiyang 550081, PR China.
E-mail address: liuchengshuai@vip.gyig.ac.cn (C. Liu).
[1] These authors contributed equally to this work.

https://doi.org/10.1016/j.jhazmat.2022.128274
Received 12 November 2021; Received in revised form 26 December 2021; Accepted 11 January 2022
Available online 13 January 2022

1. Introduction

Arsenic (As) is a well-known highly toxic metalloid. Unfortunately, contamination of soil and groundwater by As is common around the world, and it is regarded as a serious public health problem (Smith et al., 2000; Podgorski and Berg, 2020). The fate of As in the subsurface is largely controlled by iron (Fe) minerals through sorption-desorption and dissolution-precipitation cycling (Ford, 2002; Catalano et al., 2011; Karimian et al., 2017; Sowers et al., 2017). Among these Fe minerals, scorodite is most abundant and pivotal in As-contaminated acidic environments, such as acid mine drainage (AMD) and hydrometallurgical tailings (Langmuir et al., 2006; Drahota and Filippi, 2009). Scorodite deserves special attention due to its high content of As and the least soluble As phase under atmospheric conditions (Bluteau and Demopoulos, 2007; Drahota and Filippi, 2009; Zhang et al., 2021).

The stability of scorodite depends on the geochemical conditions. Under aerobic conditions, scorodite is stable at weakly acidic pH, whereas incongruent dissolution of scorodite and As release can occur under neutral to mildly alkaline conditions (Harvey et al., 2006; Bluteau and Demopoulos, 2007; Ke et al., 2019). However, dynamic redox conditions may result from seasonal fluctuations in water levels in AMD (Johnston et al., 2014). In reflood AMD environments, scorodite may be subjected to reducing conditions, which often display circumneutral pH and high concentrations of Fe(II) (Burton et al., 2008; Johnston et al., 2011). In anaerobic environments, coexisting aqueous Fe^{2+} ($Fe(II)_{aq}$) may be an important geochemical factor controlling the stability of scorodite because $Fe(II)_{aq}$ is considered a vital catalyst for the transformation of Fe oxide minerals. The interaction mechanism among Fe (II) and iron oxides was referred to electron transfer and atom exchange, resulting in dissolution of metastable Fe(III) oxides followed by reprecipitation of more thermodynamically stable phases (Pedersen et al., 2005; Handler et al., 2014; Liu et al., 2016; Frierdich et al., 2019). For example, aqueous Fe(II) can induce transformation/recrystallization of ferrihydrite into goethite, magnetite, and hematite (Hansel et al., 2003; Boland et al., 2014a; Hu et al., 2018).

In addition, the extent and rate of transformation and the identities of the mineral products are influenced by many factors, including the identity of the initial minerals (Liu et al., 2016, 2021; Karimian et al., 2017), $Fe(II)_{aq}$ concentrations (Karimian et al., 2017) and the presence of different trace metal(loid)s (Boland et al., 2014b; Liu et al., 2016; Zhang et al., 2019). Ferric-bearing minerals transformation also influence the bioavailability and mobility of trace metal(loid)s, including As. For As(V)-bearing jarosite, schwertmannite, ferrihydrite and goethite with $Fe(II)_{aq}$ (~0.5–20 mM) at pH 7.0, the presence of As hindered the transformation process (Amstaetter et al., 2010; Burton et al., 2010; Karimian et al., 2017; Zhang et al., 2019). Some studies have specifically explored the effects of this transformation process on As solid-solution partitioning and speciation, but discrepancies exist concerning the behavior of As from cases to cases. Karimian et al. (2017) reported that the addition of high Fe(II) (~20 mM) to As(V)-bearing jarosite triggered As(V) reduction to As(III), and the processes promoted As repartitioning to the surface-bound exchangeable phase. In contrast, Zhang et al. (2019) found that 50–90% of the adsorbed As was redistributed to the phosphate-unextracted phase during As-adsorbed ferrihydrite transformation induced by Fe(II). Considering that the surface chemistry of minerals can vary at the microscopic scale, this discrepancy may come from the structural characteristics of mineral or $Fe(II)_{aq}$ concentrations.

The continuous reduction of Fe(III)-bearing minerals or dissolution of Fe(II)-bearing minerals can cause the release of dissolved Fe(II). Previous studies have reported that the $Fe(II)_{aq}$ concentration in AMD sites can reach ~1.42 M in a pH range from −3.6 to neutral and can be highly dynamic with redox fluctuations (Nordstrom et al., 2000; Maillot et al., 2013). Therefore, scorodite and various concentrations of $Fe(II)_{aq}$ may coexist in these environments. Abundant $Fe(II)_{aq}$ might influence the stability of scorodite. Although a recent study reported that $Fe(II)_{aq}$ induces hydrous ferric arsenate transformed to symplesite and/or parasymplesite (Ma et al., 2021), little research has focused on the effect of $Fe(II)_{aq}$ on both the phase transition of scorodite and As behavior during the transformation process. The mineralogical characteristics of products in scorodite transformation and the consequences of As solubility and species are still unknown.

This study, therefore, aimed to investigate the effects of $Fe(II)_{aq}$ on the phase transformations of scorodite and to elucidate the speciation and partitioning of As during the transformations. The changes in mineralogy and As speciation during the phase transformations of scorodite with different $Fe(II)_{aq}$ concentrations were concurrently traced using complementary techniques, including selective extractions, X-ray diffraction (XRD), ^{57}Fe Mössbauer spectroscopy, X-ray absorption spectroscopy (XAS), X-ray photoelectron spectroscopy (XPS), and transmission electron microscopy (TEM). These discoveries are expected to further the understanding of the geochemical behavior of arsenic during scorodite transformation in natural environments.

2. Materials and methods

2.1. Scorodite synthesis

Scorodite was synthesized using a hydrothermal process modified from Kossoff et al. (2015). Briefly, concentrated HCl (37%) was used to acidify an As(V)-bearing solution (from $Na_2HAsO_4{\cdot}7H_2O$) to pH 1.0. Once the target pH value was reached, the solution was heated to 95 °C. 100 mL of 0.2 M Fe(III) stock solution (prepared from $FeCl_3{\cdot}6H_2O$) was then added slowly with a peristaltic pump at a rate of 100 mL/h and the mixture was stirred for 24 h. Subsequently, the suspension was transferred into a stainless steel autoclave with PTFE liners and put at 150 °C in an oven for 48 h. The suspension was centrifuged after cooling to room temperature. The solid was cleaned by Milli-Q water at least three times. The final solid was dried at 50 °C in an oven for 24 h and then stored in a desiccator for further experiments.

2.2. Transformation experiments

A batch incubation method, as described by Liu et al. (2021), was used to study the phase transformation of scorodite in the presence of Fe (II). All preparations and experimental runs were carried out in an anaerobic glovebox (COY, Type C) with palladium catalyst (O_2 consumption) and ~8% H_2 in a N_2 atmosphere. All solutions were deoxygenated with N_2 for at least 4 h prior to transferring into the anoxic glovebox. The anerobic atmosphere need at least 24 h to equilibrate. Iron powder was dissolved in 4 M HCl with magnetic stirring overnight in a glovebox and diluted with deoxygenated Milli-Q water to achieve 100 mM Fe(II) stock solution.

Four $Fe(II)_{aq}$ concentrations of 0 (control), 1, 5, and 10 mM were attained by diluting the Fe(II) stock solution. The molar ratio of the highest concentration of Fe(II) (10 mM) to structural Fe(III) (8.7 mM) was ~1.2, which was deemed representative of those found in AMD (Fe (II)/Fe(III) molar ratio of ~1.1) (Burton et al., 2011). The Fe(II)-bearing solutions were buffered with 4-(2-hydroxyethyl)-1-piperazineethane-sulfonic acid (HEPES) (30 mM, pH 7.0). The pH adjustments were achieved with anaerobic HCl and NaOH solutions in an anoxic chamber. Then, the reaction was initiated by adding 20.0 ± 0.5 mg of scorodite to ~10 mL pre-equilibrated Fe(II)-bearing solutions. These 15 mL centrifuge tubes were wrapped with aluminum foil and placed on a rolling oscillator, which was placed inside the anaerobic chamber. The total duration of this experiment was 600 h, during which the reactors were opened for subsampling at prescribed time intervals (i.e., 4, 24, 120, 240, 340, 480, 600 h). Triplicates were prepared for all experiments.

During subsampling, the Eh and pH of each treatment were measured using a HACH HQ40d meter. The suspension samples were collected from each treatment and centrifuged (9500 rpm, 10 min). The supernatant was filtered through 0.45-μm hydrophilic syringe filters and

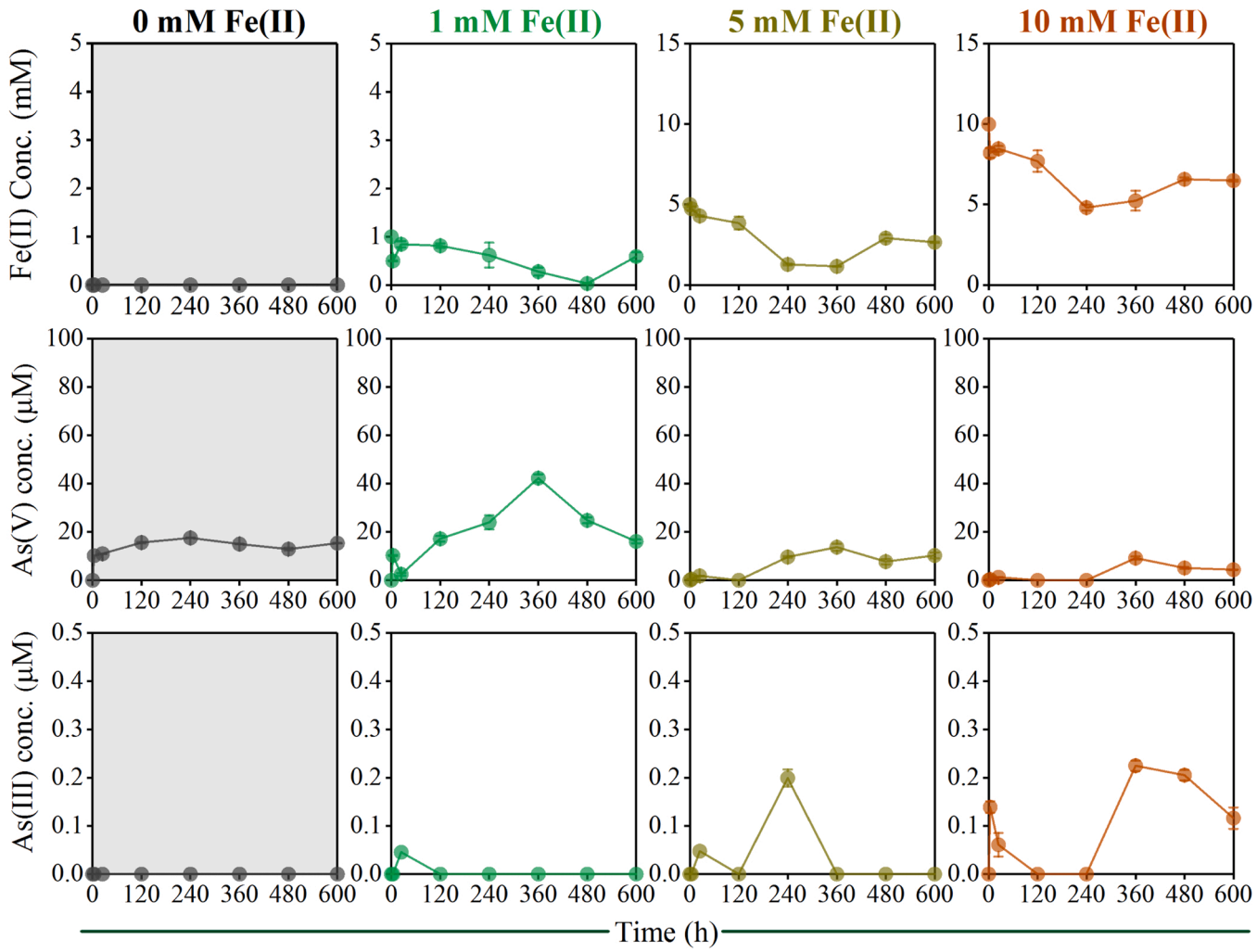

Fig. 1. Aqueous concentrations of Fe(II), As(V) and As(III) in different Fe(II) concentration treatments over 600 h. The standard deviations of triplicate subsamples are shown by the error bars.

acidified with 50 μL of 5 M HCl for dissolved Fe(II), As(V) and As(III) concentration analysis. The solid was then resuspended in 10 mL of 1 M KH_2PO_4 and shaken for 6 h. The centrifuged supernatant was filtered and analyzed to determine the concentration of surface adsorbed As (phosphate-extractable) (Zhang et al., 2019). Then, the residual solid was resuspended in 1 M HCl (10 mL) and shaken for 4 h. The centrifuged supernatant was filtered and analyzed to determine the concentration of As combined with poorly crystalline Fe minerals (Karimian et al., 2017). Finally, the residual solid was digested in 5 M HCl to determine total Fe [$Fe(T)_s$] and total As [$As(T)_s$] (Hua et al., 2019; Y.N. Liu et al., 2018; Zhang et al., 2019).

To further investigate the Fe phase transformation, another experiment involving treatments of scorodite with 10 mM $^{57}Fe(II)_{aq}$ was conducted using the same procedures as above. The $^{57}Fe(II)$-enriched stock solution was prepared by dissolving $^{57}Fe(0)$ powder (95.08% ^{57}Fe, Isoflex, USA) in 4 M HCl. After the reaction, the residual solids were isolated on a 0.45-μm hydrophilic filter membrane and dried in an anaerobic chamber. Then, the membrane with reacted solid was fixed between two pieces of polyimide tape and stored in the anaerobic chamber until analysis with Mössbauer spectrometry.

2.3. Solution analyses

The concentrations of total Fe and As in the acid digests of the residual solids were measured by a PerkinElmer Optima 8000 inductively coupled plasma optical emission spectrometer (ICP-OES, USA). The concentrations of Fe(II) and total Fe were determined by the ferrozine method at 510 nm. Hydroxyl ammonium chloride solution (100 g/L), as a reducing agent, was added for total Fe determination. The differences between Fe(T) and Fe(II) were calculated to determine the Fe(III) concentration. Arsenic species concentrations were determined by liquid chromatography coupled to an atomic fluorescence spectrometer (LC-AFS, AFS-9700, Jitian, Beijing) with a detection limit of 0.5 μg/L (Hua et al., 2022).

2.4. Solid phase analyses

XRD was used to assess the mineralogy of the solids. The XRD patterns were collected using an X-ray diffractometer (XRD, D2, Bruker, Germany) equipped with a Co Kα radiation source (36 kV and 36 mA). The XRD patterns were collected at 0.02° (2θ) step size over a range from 10° to 80° (2θ) with a scanning rate of 1 s per step. Phase recognition was accomplished by comparing the attained patterns with the standard mineral diffraction database (JCPDS PDF-2 database) (Liu et al., 2021). Quantitative analysis was employed with the Rietveld method described by Perl et al. (2012) using TOPAS V5 software (Bruker AXS, Germany).

The morphologies and elemental compositions of the solids were observed using transmission electron microscopy (TEM, Tecnai F20). For energy dispersive spectroscopy (EDS) mapping, the elemental distributions of Fe, O and As in the selected samples were analyzed by an

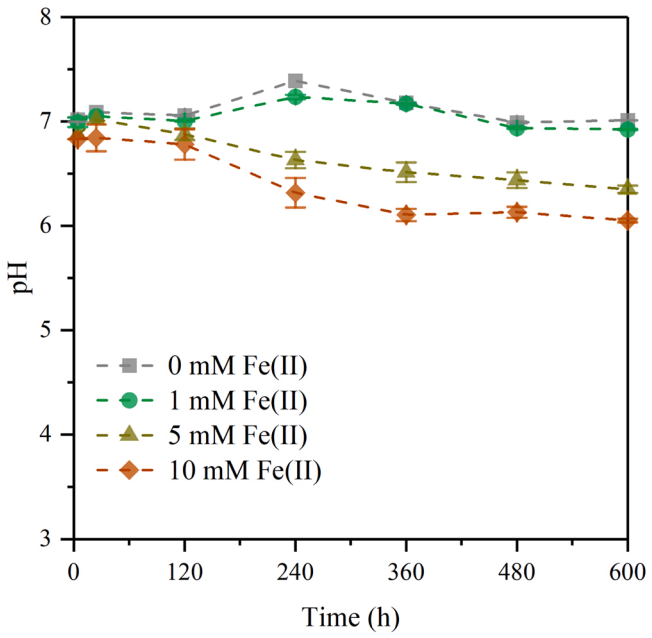

Fig. 2. Temporal changes in pH during the transformation of scorodite in the presence of different Fe(II) concentrations over 600 h. Standard deviation of triplicate subsamples are shown by the error bars.

FEL Talos F200X. The samples were prepared by ultrasonic dispersion with ethanol, and a few drops of suspension were pipetted onto an ultrathin carbon film, which was supported by a 200-mesh copper grid. Then, the samples were analyzed under higher vacuum at 200 kV.

^{57}Fe Mössbauer spectra of selected solid samples were collected with a Wissel Elektronik (Germany) instrument, performed in transmission mode with a ^{57}Co (~50 mCi) source at room temperature (RT, ~298 K). Data were calibrated by α-Fe(0) foil and fitted using MössWinn 4.0 software, following the reported method (Neumann et al., 2013).

The valence state of As on the surface of scorodite was measured by X-ray photoelectron spectrometer (XPS, Thermo Scientific NEXSA). All XPS patterns were acquired by setting the pass energy of broad scans to 100 eV and narrow scans to 50 eV. Narrow scans for As 3d were performed with XPS peak 41. To further explore the oxidation states of As and the bonding between As and the Fe phases, As K-edge X-ray absorption spectra (XAS) were recorded at beamlines 20-BM at the Advanced Photon Source (APS; Illinois, USA). Na_3AsO_3 and $Na_2HAsO_4{\cdot}7H_2O$ were used as references. X-ray absorption near-edge structure (XANES) data analyses were completed in ATHENA (Ravel and Newville, 2005), including energy calibration, edge-step normalization, and subtraction of a spline background. Artemis was used to analyze extended X-ray absorption fine-structure (EXAFS) data following the method described by Feng et al. (2020). Getting the crystallographic information file of reference materials from the American Mineralogist Crystal Structure database (AMCSD), which were used as theoretical models in EXAFS fitting. Obtaining the amplitude reduction factor (S_0^2) from refinement for the first shells of scorodite with a fixed coordination number (*CN*). The value of S_0^2 was then considered a constant during the refinement of shells of unknown samples to obtain *CN*, Debye-Waller factors (σ^2), and interatomic distances (ΔR). All EXAFS spectra were fitted for *CN*, ΔR, σ^2, and energy difference (ΔE) between selected and theoretical E_0 in the 3–10 Å^{-1} range. A k weighting of 3 was applied to enhance weak oscillation in the far end of the EXAFS spectra. The results for the *R*-factor, *CN*, and ΔR were then used to evaluate the best-fit results (P. Liu et al., 2018; Feng et al., 2020).

3. Results and discussion

3.1. Temporal variations in aqueous Fe and As

In all Fe(II)-bearing treatments, the concentrations of dissolved Fe(II) sharply decreased after approximately 4 h (Fig. 1), which can be attributed to adsorption of Fe(II) onto the minerals by forming complexes (Pedersen et al., 2005; Boland et al., 2014a). Dissolved Fe(II) decreased firstly and then increased toward the end of experiment in all Fe(II)-bearing treatments. This might be ascribed to the dissolution of Fe(II)-bearing minerals formed in these systems. The concentrations of dissolved Fe(II) were equal to the dissolved total Fe (Fig. S1). Therefore, dissolved Fe(III) concentrations remained low. In the Fe(II)-free control,

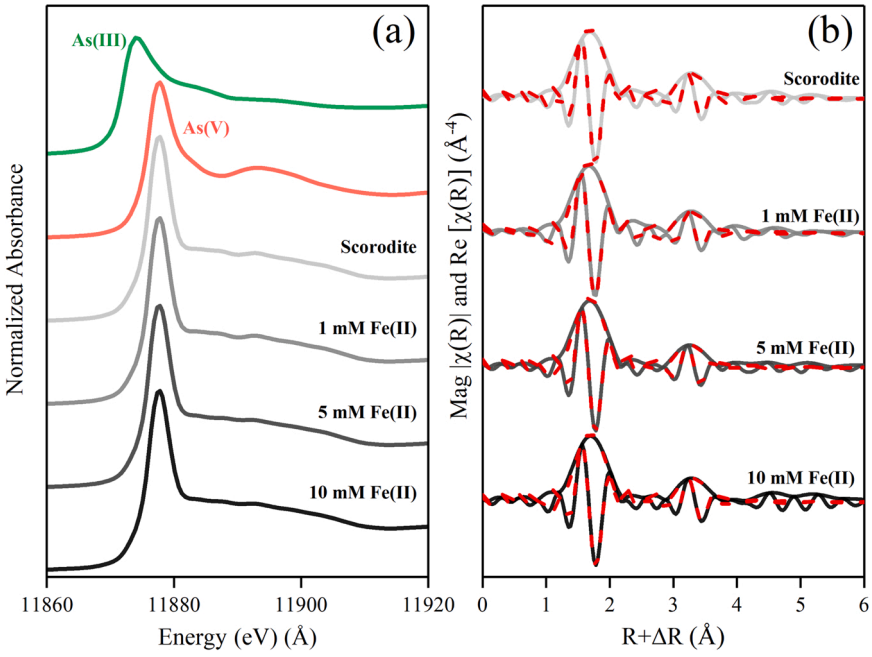

Fig. 3. (a) Arsenic K-edge XANES, (b) Magnitude and real part of the corresponding Fourier transform for samples with different Fe(II) concentrations after 480 h. The solid lines indicate measured data, whereas the red dash shows the resulting fit.

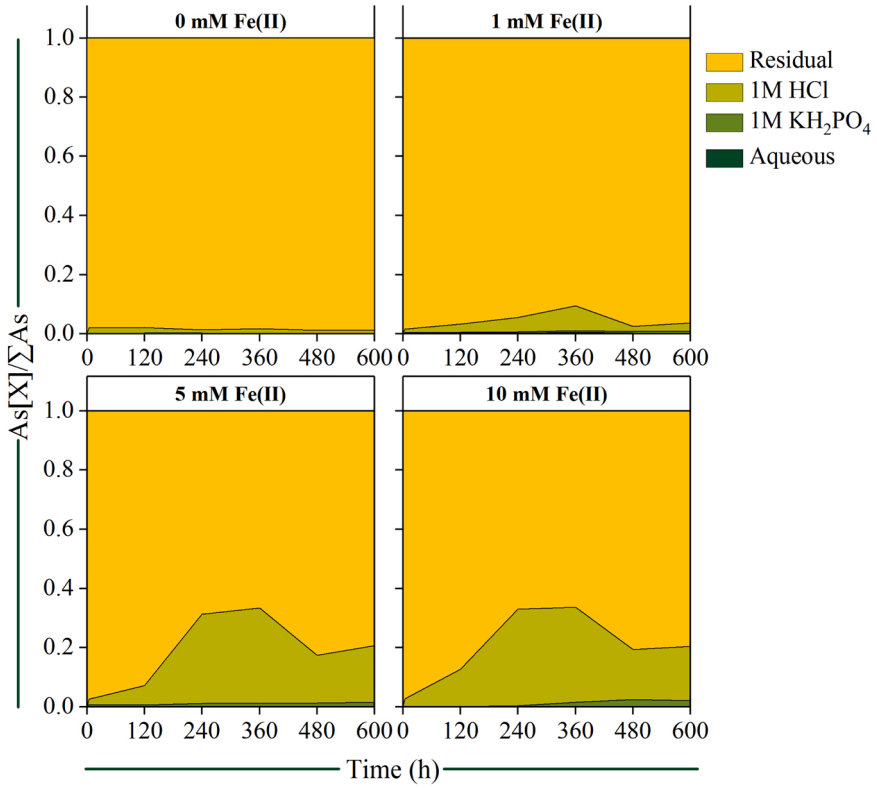

Fig. 4. Solid-phase distribution of As during transformations of scorodite at pH 7.0 in different Fe(II) concentration treatments over 600 h. The data are represented as a proportion of total As.

Table 1
Shell fitting parameters for scorodite samples before and after reaction with 1, 5, and 10 mM Fe(II).

Sample	Path	*CN*	*R*(Å)	σ^2(Å^2)	ΔE_0(eV)	*R*-factor
Before	As-O	4.0(9)	1.67(1)	0.001	2.6(2.9)	0.027
	As-O-O	**12**	3.05			
	As-Fe	3.0(7)	3.35(1)	**0.004**		
1 mM Fe(II)	As-O	4.3(3)	1.68(1)	**0.001**	1.7(2.5)	0.025
	As-O-O	**12**	3.06			
	As-Fe	3.2(8)	3.35(0)	**0.006**		
5 mM Fe(II)	As-O	3.9(7)	1.68(1)	0.002	2.9(2.5)	0.020
	As-O-O	**12**	3.06			
	As-Fe	3.4(8)	3.34(1)	**0.006**		
10 mM Fe(II)	As-O	3.8(9)	1.68(1)	0.001	4.2(2.8)	0.029
	As-O-O	**12**	3.06			
	As-Fe	3.6(9)	3.36(1)	**0.006**		

CN: coordination number (path degeneracy); σ^2: Debye-Waller factor; *R*: modeled bond length; ΔE_0: energy shift from the calculated Fermi level; *R*-factor: goodness-of-fit parameter. The As-O-O paths ($R = 1.82R_{\text{As-O}}$, $\sigma^2 = \sigma^2_{\text{As-O}}$) improved the fits but unmodified the results for other shells concerning the estimated errors. The amplitude reduction factor ($S0^2$) was 1.0. All EXAFS spectra were fitted from 1 to 3.7 Å in R space. $N_{\text{idp}} = 11.8$, and $N_{\text{var}} = 5$–6. Bold values were fixed to the anticipated value.

dissolved Fe(II) and total Fe were both undetectable (Figs. 1 and S1). Similar results also appeared in previous studies and were attributed to incongruent scorodite dissolution to ferrihydrite at neutral pH (Harvey et al., 2006; Paktunc and Bruggeman, 2010).

The concentrations of dissolved As(V) increased over time in both the control and all Fe(II) treatments (Fig. 1). In the Fe(II)-bearing treatments, the concentrations of dissolved As(V) were dependent on the initial $Fe(II)_{aq}$ concentrations, which decreased with increasing of $Fe(II)_{aq}$ concentrations. Addition of 1 mM $Fe(II)_{aq}$ followed an increase in dissolved As(V) within ~360 h, reached the maximum value of ~43 μM, and then decreased to ~20 μM at the end stage of the experiment (Fig. 1). The observed increase in As(V) indicated that the addition of Fe (II) enhanced the dissolution of scorodite. However, the observed drop in As(V) concentrations might be ascribed to both surface adsorption and incorporation into the neo-formed secondary Fe minerals (Fig. S1). Previous studies have reported that scorodite dissolves incongruently, producing iron hydroxide so that the dissolved As may adsorb to its surface (Langmuir et al., 2006). Although the dissolved As(V) concentrations increased over time, they were low during the first 120 h and the maximum values were only ~14 μM and ~10 μM in the 5 and 10 mM Fe(II) treatments, respectively. It should be noted that the pH decreased by 0.7–0.8 pH units in the presence of 5 and 10 mM Fe(II) even with pH buffer solution (Fig. 2), indicating that the dissolution reaction was enhanced by high concentrations of Fe(II). At pH ≥ 3.0, the incongruent dissolution of scorodite can produce hydrogen ions, causing a decrease in pH (Harvey et al., 2006). The pH decrease may be obligated to the observed enhanced As(V) sequestration at higher Fe (II)-bearing treatments.

Previous research has reported that the transformations of Fe(III) oxides induced by Fe(II) can trigger As(V) reduction (Karimian et al., 2017; Perez et al., 2019; Wang et al., 2020). This phenomenon also occurred in our study, with the greatest reduction occurring in the presence of 10 mM Fe(II) (Fig. 1). The concentration of dissolved As(III) increased from 0 to 0.22 μM within ~360 h and decreased to 0.11 μM at the terminal stage of the experiment in the presence of 10 mM Fe(II). In the l and 5 mM Fe(II) treatments, after achieving maximum values of ~0.05–0.20 μM, As(III) rapidly decreased to the detection limit. In the Fe(II)-free control, dissolved As(III) was undetectable.

3.2. *As speciation and solid-solution partitioning*

XPS and XANES analyses were used to identify the valence state of solid phase As. Both techniques showed that As(V) remained in its oxidation state during Fe(II)-induced scorodite transformation (Fig. 3a

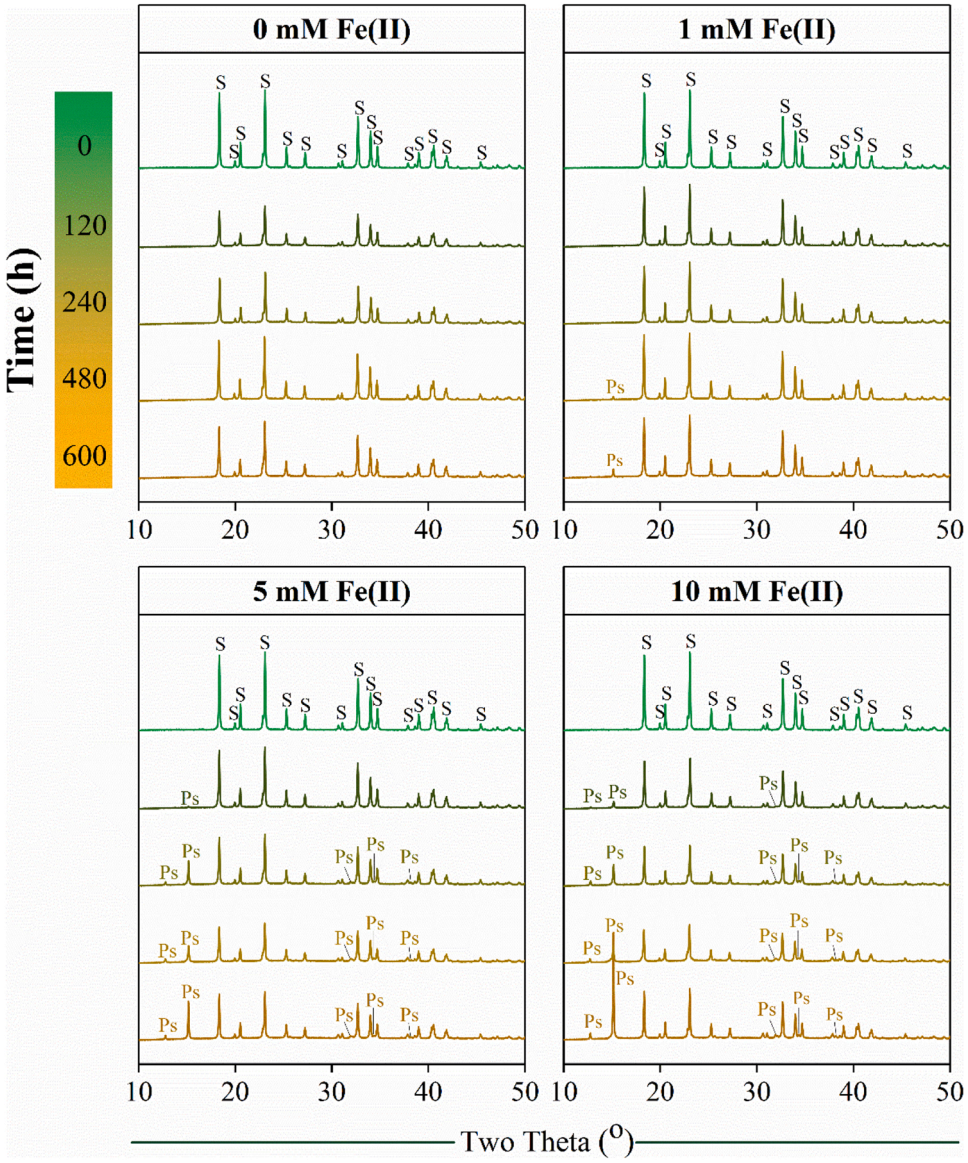

Fig. 5. XRD patterns for the precipitates formed during the reaction of scorodite with different Fe(II) concentrations over 600 h. S-scorodite ($FeAsO_4{\cdot}2H_2O$) and Ps-parasymplesite [$Fe_3(AsO_4)_2{\cdot}8H_2O$].

and Fig. S2). Karimian et al. (2017) found that ~26% abiotic reduction of As(V) occurred only at a high molar ratio of Fe(II)/As(V) (~260) during the transformation of jarosite. This phenomenon has been observed in ferrihydrite transformations with high Fe(II)/As(V) molar ratios from 15.6 to 62.6 (Perez et al., 2019). In our study, the value of Fe (II)/As(V) was ~1.16 and therefore much lower. Combined with the results of the aqueous phase (Fig. 1), reduced As(III) could be released into solution due to its higher mobility and lower affinity for secondary Fe phases than As(V) under circumneutral conditions (Cummings et al., 1999; Johnston et al., 2012; Revesz et al., 2015; Chai et al., 2016; Zhou et al., 2018). Of course, the content of As(III) was lower than detection limit if it existed.

To assess the As (re)distribution during scorodite transformation, the proportions of As in the aqueous, adsorbed (PO_4^{3-}-extractable), 1 M HCl-extractable, and residual fractions were determined (Fig. 4). Aqueous As concentrations were always below 0.5% of the total As in all treatments, which indicated that As was mainly stable in the solids. The fraction of PO_4^{3-}-extractable As increased slightly with increasing $Fe(II)_{aq}$ concentration over the reaction period. Approximately 2.4% of the total As was PO_4^{3-}-extractable, suggesting that As was re-adsorbed on the neo-formed Fe(III) oxides surface. In addition, the proportion of 1 M HCl-extractable As increased from ~1.2–2.5% to ~9–33% in the addition of Fe(II), implying that As might be distributed to the poorly crystalline Fe oxides. The PO_4^{3-}-extractable and 1 M HCl-extractable fractions of As were greater in the 5 and 10 mM Fe(II) treatments. In contrast, the surface absorbed and 1 M HCl-extractable fractions of As remained relatively invariable in the Fe(II)-free treatments. The elevated fractions of surface-adsorbed As and the fraction of poorly crystalline secondary Fe mineral-associated seemed to coincide with partial phase transformation of scorodite. Additionally, the results showed that the solubility of As decreased with increasing Fe(II) concentrations. The As solubility was negligible at high Fe(II) concentrations, suggesting that the released structure As(V) was quickly sequestered by the neo-formed Fe minerals. Similar trends of decreasing As solubility occurring on the formation of various Fe oxides, (e.g., ferrihydrite, goethite, and Fe(II)-As (V) minerals) have also been reported in previous studies (Karimian et al., 2017; Zhang et al., 2019; Ma et al., 2021).

The coordination environment of As was explored by shell fitting of the EXAFS data (Fig. 3b and c). The fitting *R*-factors ranged from 0.020 to 0.029, which indicated that the fits were reasonable (Table 1). For all

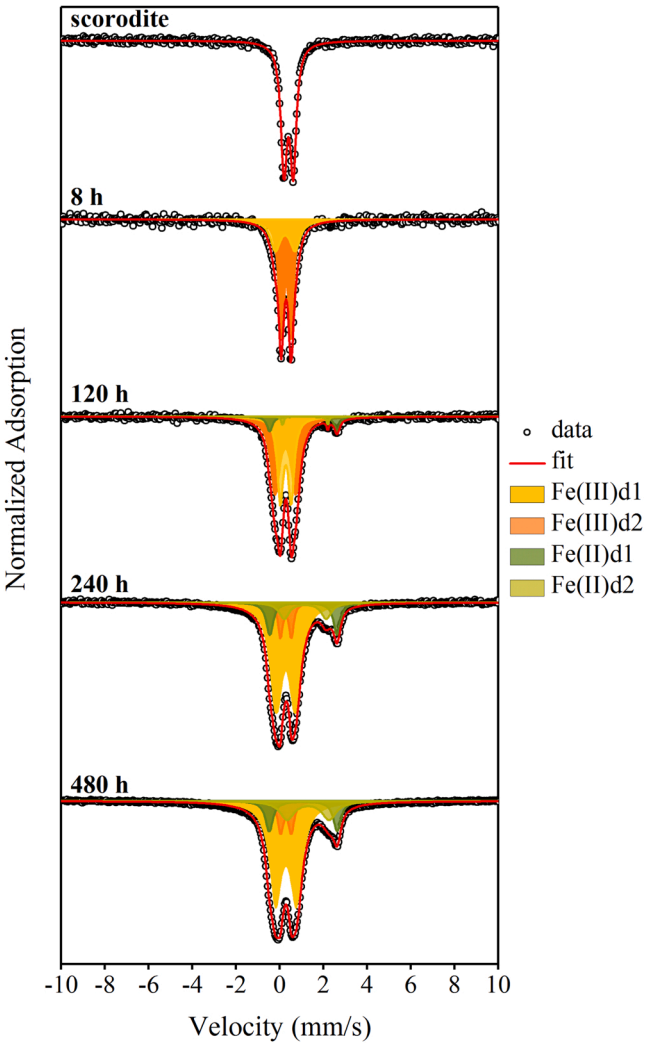

Fig. 6. Mössbauer spectra of scorodite before and after exposure to 10 mM aqueous ^{57}Fe(II) at room temperature (~298 K).

samples, the first shell at a distance of 1.67 ± 0.01 Å with a coordination number (*CN*) of 4.0–4.3 corresponds to AsO_4 tetrahedra (Mikutta et al., 2013). These results further suggested that no As(III) species were detected, which would be characterized by an As-O distance of 1.79 Å with a *CN* of 3.0 (Manning et al., 1998; Randall et al., 2001). Second coordination shell contributions to the EXAFS data were fitted by the As-Fe pairs at 3.34–3.36 Å together with multiple scattering (MS) matching the As-O-O paths within the AsO_4 tetrahedra (Table 1). The *CN* of the As-O-O paths was fixed at 12. The EXAFS spectra of the sample before reacting with $Fe(II)_{aq}$ showed that 3.0 Fe atoms surrounded the As at 3.35 Å, consistent with the structure of scorodite (Mikutta et al., 2013). After reacting with $Fe(II)_{aq}$ for 480 h, the As-Fe distance remained unaltered, but the *CN* of As-Fe increased from 3.2 to 3.6 when the concentration of $Fe(II)_{aq}$ increased from 1 to 10 mM. The increase in $CN_{As\text{-}Fe}$ would be ascribed to the additional As-Fe pair of the precipitated secondary As-bearing Fe mineral (Perez et al., 2020). These results indicated that inner-sphere complexes of dissolved As(V) formed (Wang and Mulligan, 2008) and further confirmed As repartitioning in the presence of $Fe(II)_{aq}$.

3.3. Phase transformation of scorodite

Reacted products of the minerals were characterized at different sampling times for the four treatments (Fig. 5). For the Fe(II)-free treatment, the XRD patterns showed no significant changes in mineralogy over the experimental period. However, parasymplesite [$Fe_3(AsO_4)_2{\cdot}8H_2O$] was detected for all three aqueous Fe(II) treatments, suggesting that Fe(II) reacted with scorodite and induced scorodite transformation to the secondary Fe(II)-As(V) phase. Moreover, discrepancies between XRD patterns suggested that the rates of transformation increased as the initial Fe(II) concentration increased. For the 1 mM Fe(II) treatment, XRD patterns obtained after 480 h exhibited a weak peak at approximately 15.2° (2θ), which is assigned to parasymplesite (Revesz et al., 2015). The final dominant Fe phases were scorodite (99.25%) with a minor amount of parasymplesite (~0.75%) (Figs. 5 and S3). Compared to those of 1 mM Fe(II), the transformation was faster in the presence of 5 and 10 mM Fe(II), and the characteristic peaks of parasymplesite occurred within 120 h of reaction. Scorodite (~87.1–88.5%) and parasymplesite (~11.5–12.9%) were the dominant phases at the end of the experiments (Fig. S3).

Mössbauer spectroscopy is more sensitive than XRD, which facilitates the identification of both low abundance and amorphous iron oxides in solids. Mössbauer spectra of scorodite before and after reaction with 10 mM ^{57}Fe(II) were employed at 298 K (Fig. 6 and Table S1). After the addition of ^{57}Fe(II) for 8 h, the spectra were fit by two distinct Fe(III) doublets with values of quadrupole splitting (*QS*, 0.45–0.95 mm/s) and isomer shift (*IS*, 0.25–0.29 mm/s) (Table S1). Fe(III)d1 (*IS* = 0.25–0.28 mm/s, *QS* = 0.88–0.95 mm/s) is broadly consistent with 2-line ferrihydrite-like minerals (Cornell and Schwertmann, 2003). Fe(III)d2 (*IS* = 0.27–0.29 mm/s, *QS* = 0.45–0.50 mm/s) is consistent with scorodite (Gallup and Mreiff, 1991; Mikutta et al., 2014). Two distinct Fe(II) doublets appeared in the samples with values of ~1.07–1.29 mm/s for *IS* and ~1.92–3.11 mm/s for *QS* after reacting for 120 h, which were assigned to parasymplesite. The amount of parasymplesite and ferrihydrite-like species present in solids increased to 26.1% and 64.7%, respectively, and this was accompanied by a decrease in scorodite (Fig. S4).

Fe(II) interact with structural Fe(III)/As(V) might have resulted in different rates of scorodite transformation. Increasing the concentration of Fe(II) is likely to enhance the surface complexation of Fe(II) with the limited surface sites of minerals and accelerate electron transfer to structural Fe(III) or As(V) (Karimian et al., 2017). The initial mineral rapidly dissolved and transformed to a more thermodynamically stable phase, which could be driven by accelerated electron transfer (Cornell and Schwertmann, 2003; Karimian et al., 2017). According to PHREEQC thermodynamic calculations of the solubilities of scorodite (K_{sp} = $10^{-22.59}$) (Robins, 1987) and parasymplesite ($K_{sp} = 10^{-33.25}$) (Johnston and Singer, 2007) as a function of pH, parasymplesite was more stable under near-neutral pH conditions.

The formation of parasymplesite and ferrihydrite-like structures was also verified by TEM. Distinctive elongated tabular shards, rod-like and cotton-like structures occurred in 5 and 10 mM Fe(II) batches (Fig. 7b–f). After reacted with Fe(II), the structure of scorodite was destructed and the smooth surface particles (Fig. S5) were changed to a mixture of nonsmooth shapes (Fig. 7). This is possible due to the reductive dissolution of scorodite, which further resulted in the formation of new secondary minerals with particular morphology. EDX analysis showed elongated tabular shard and rod-like particles with Fe/As molar ratios ranging from 1.57 to 1.77 (Fig. 7e, f and Table 2), implying that secondary parasymplesite phases (Fe/As = 1.5) were produced and that some Fe accumulated around the minerals. The cotton-like aggregate exhibited high Fe/As (2.05–5.14) due to the formation of a considerable amount of ferrihydrite-like species and dissolved As adsorbed on its surface (Mandaliev et al., 2013). In the 1 mM Fe(II) treatment, the Fe/As molar ratios on the edges of the particles were 2.07, implying that a considerable amount of Fe accumulated around the solid and that could reduce the mobility of dissolved As (Fig. 1). In line with the XRD and Mössbauer results (Figs. 5 and 6), considerable amounts of tabular shard/rod-like and cotton-like aggregate minerals formed in the presence of 5 and 10 mM Fe(II), resulting in

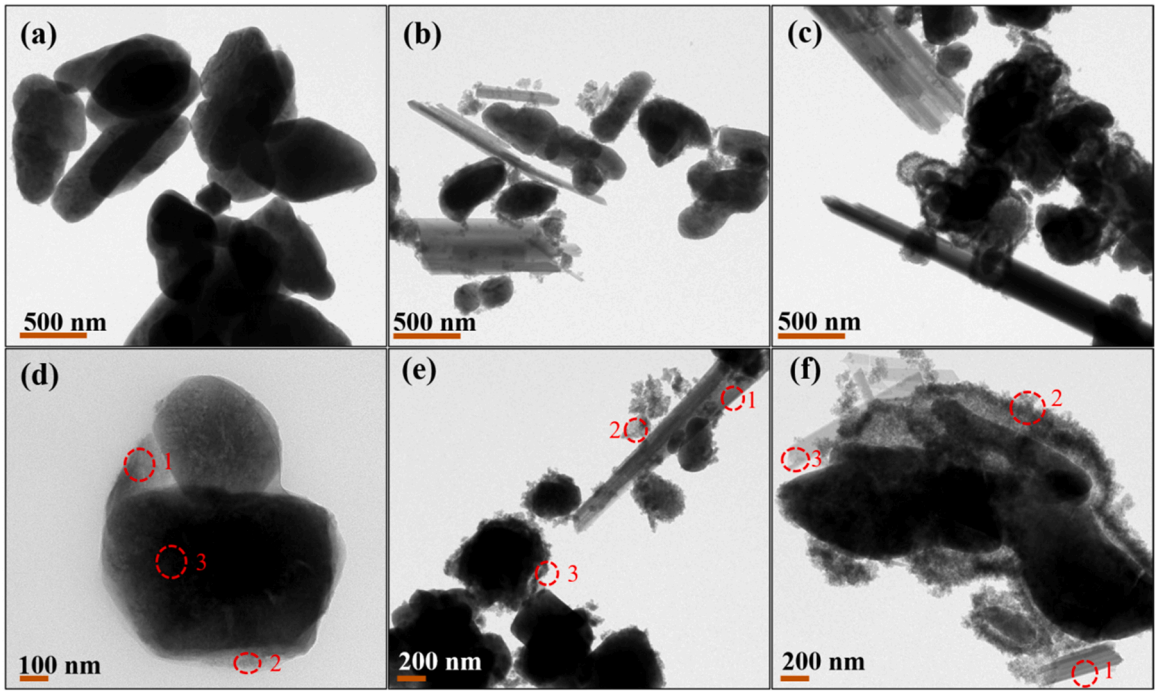

Fig. 7. TEM images of scorodite after 600 h of exposure at pH 7.0 to (a, d) 1 mM Fe(II), (b, e) 5 mM Fe(II), and (c, f) 10 mM Fe(II). The red circles indicate the spots analyzed for elements by TEM-EDX.

Table 2
Elemental contents obtained from TEM-EDX for spots indicated with red circles are shown in Fig. 7.

Sample	Spot	Content/at%		Fe/As molar ratio
		Fe	As	
1 mM Fe(II)	1	13.40	12.97	1.03
	2	10.04	4.85	2.07
	3	12.75	12.36	1.03
5 mM Fe(II)	1	19.02	12.15	1.57
	2	28.12	8.76	3.21
	3	25.22	4.66	5.41
10 mM Fe(II)	1	16.73	9.45	1.77
	2	28.79	6.93	4.15
	3	35.19	17.13	2.05

a decrease in dissolved As and an increase in HCl-extractable As (Fig. 4). No other different morphology formed suggest that the conversion of ferrihydrite-like to crystalline Fe (oxyhydr)oxides did not occur in the present study, and it is possible that a high content of As inhibits the process (As/Fe molar ratio of ~0.98). Similar results of inhibited transformation of ferrihydrite to more stable minerals such as goethite and magnetite have been reported in previous research (As/Fe molar ratio of ~0.025) (Zhang et al., 2019; Hu et al., 2020).

To directly observe the distribution of As on secondary mineral phases, we employed high-angle annular dark field (HAADF) scanning transmission electron microscopy (STEM) analyses. HAADF-STEM images of scorodite reacted with 10 mM Fe(II) revealed a bright area in the aggregates, which was separated from the elongated plates (Fig. 8b). The EDS maps revealed that Fe, O and As were nearly homogeneously distributed across the parasymplesite crystal (Fig. 8c–f). The high distributions of Fe and O led to brightness and a trace amount of As accumulated, which corresponded to the adsorption of As on the ferrihydrite-like surface. The STEM-EDS results have provided visual evidence of As distribution on secondary minerals. These results cross-correlate and confirm the observations from EXAFS and chemical extractions and suggest that the increase in $CN_{As\text{-}Fe}$ was indeed due to an additional As-Fe pair in the secondary As-rich precipitates of parasymplesite and ferrihydrite-like species (Wang et al., 2011; Perez et al., 2020).

3.4. Mechanisms for the mobilization of arsenic during transformation

According to the above results, the solubility of As was strongly dependent on its redistribution in solids, including dissolution of unreacted As-bearing iron (oxyhydr)oxides, formation of secondary minerals, and sorption-desorption of As on these mineral surfaces (Fan et al., 2019; Wang et al., 2020; Yu et al., 2020). The participation of Fe $(II)_{aq}$ accelerated the reductive transformation of scorodite. The possible mechanism of phase transformation of scorodite involved electron transfer among added $Fe(II)_{aq}$, solid Fe(III) and As(V) at the liquid–solid interface (Cornell and Schwertmann, 2003; Karimian et al., 2017). The electron transfer between solid Fe(III) is the main driver of scorodite dissolution, and subsequently, the dissolved Fe(III) was precipitated as Fe(III)-bearing species such as ferrihydrite (Eq. (1)). The transformation processes triggered rapid, minor As (< 0.5%) mobilization into the aqueous phases. In the 1 mM Fe(II) treatment, dissolved As(V) was adsorbed on or incorporated into the neo-formed ferrihydrite-like species after aging for 600 h (Eq. (2)), which contributed significantly to As sequestration (Fig. 1).

$$FeAsO_4{\cdot}2H_2O + H_2O \rightarrow HAsO_4^{2-} + Fe(OH)_3(s) + 2H^+ \quad (1)$$

$$As(V) + \equiv Fe(OH)_3(s) \rightarrow As(V) \equiv Fe(OH)_3(s) \quad (2)$$

The fact that As mobilization was low in the high Fe(II) concentrations suggests that the released structural As(V) was quickly adsorbed on the surfaces or incorporated into the structures of the new-formed Fe phases, e.g., amorphous ferrihydrite-like and parasymplesite species, depending on experimental conditions. When the addition of $Fe(II)_{aq}$ was increased, the reactions between dissolved As(V) and Fe(II) occurred, as in Eq. (3), and therefore leads to a surface precipitation of parasymplesite. The indirect formation of parasymplesite consists of the release of As(V) from scorodite dissolution (Eq. (1)) and precipitation with aqueous Fe(II) (Eq. (3)). In addition, part of scorodite can react

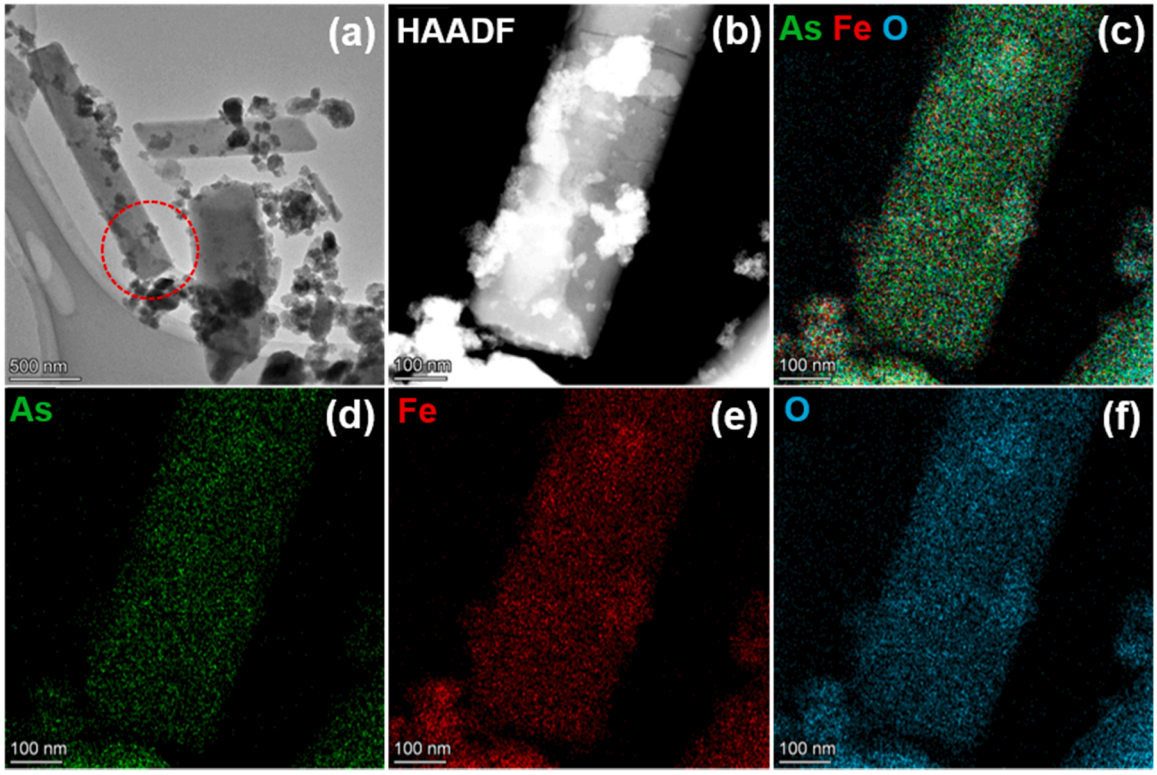

Fig. 8. (a) TEM image of scorodite reacted with 10 mM Fe(II). (b) HAADF-STEM image of the red dotted circle in (a) and corresponding EDX elemental maps: (c) combined As, Fe, O; (d) As (green); (e) Fe (red); (f) O (cyan).

directly with the dissolved Fe(II) and produce parasymplesite (Eq. (4)). Oxidized Fe(III) was hydrolyzed to a ferrihydrite-like product, and the dissolved As was adsorbed on the surface. These secondary phases may either coat or isolate from scorodite, causing surface passivation that retards the release of arsenic or sequesters the dissolved arsenic (Figs. 1 and 7).

$$3Fe^{2+} + 2HAsO_4^{2-} + 8H_2O \rightarrow Fe_3(AsO_4)_2 \cdot 8H_2O(s) + 2H^+ \quad (3)$$

$$3Fe^{2+} + 2FeAsO_4 \cdot 2H_2O + 10H_2O \rightarrow Fe_3(AsO_4)_2 \cdot 8H_2O(s) + 2Fe(OH)_3(s) + 6H^+ \quad (4)$$

In our experiment, high concentrations of Fe(II) (5 and 10 mM) enhanced the incongruent dissolution of scorodite to form ferrihydrite-like and arsenate oxyanions ($HAsO_4^{2-}$ or $H_2AsO_4^-$), producing hydrogen ions (Eq. (1)). Additionally, the dissolved As(V) adsorbed on the ferrihydrite-like specie and precipitation of parasymplesite also yield hydrogen ions (Eqs. (2) and (3)), causing a decrease in pH (Fig. 2). Thus, incongruent dissolution of scorodite enhanced by Fe(II) and As sequestered on secondary Fe minerals should lower the pH.

It is remarkable that As(V) reduction occurred during the Fe(II)-induced scorodite transformation, and this reduction was enhanced by increases in $Fe(II)_{aq}$ concentrations (Fig. 1). Previous studies reported that As(V) reduction was triggered by the Fe(II)-goethite redox couple during the Fe(II)-induced transformation of As(V)-bearing ferrihydrite and jarosite (Karimian et al., 2017; Perez et al., 2019). It must be noted, however, that goethite was not formed in our study. This revealed that another one existed and may have triggered the reduction of As(V). Although little research has reported that the surface-adsorbed Fe(II) and ferrihydrite-like redox couple can induce As(V) reduction, it is a most likely candidate because ferrihydrite-like specie was the major final product (~65%) formed with higher Fe(II) concentrations in our study (Fig. S4). In addition, the electron, which remained in the conduction band, could react with As(V) and result in the reduction of As(V) to As(III). However, no As(III) was detected in the solid, perhaps because As(III) had a weaker affinity for Fe(III)-bearing minerals than As(V) and was incapable of precipitating with Fe(II) at neutral pH (Tian et al., 2017). Additionally, Fe(II) is able to compete for the surface site on the neo-formed ferrihydrite-like phase. Therefore, during the transformation of scorodite in Fe-rich environments, As(V) may be repartitioned in secondary Fe minerals, while reduced As(III) may be released.

4. Conclusions

In this study, Fe(II)-induced transformation of scorodite under anaerobic conditions was studied. The results showed that ferrihydrite-like and parasymplesite species were formed during the Fe(II)-induced scorodite transformation, and the extent of transformation increased with increasing Fe(II) concentrations. Moreover, our study showed that the solubility and species of As changed with the transformation of scorodite. A considerable amount of structural As(V) was redistributed into extractable phases during the scorodite transformation, and the fraction of the extractable phase increased with increasing Fe(II) concentration. The immobilization of As may have involved adsorption or incorporation by neo-formed parasymplesite and ferrihydrite-like minerals during the transformation process. Additionally, this study also disclosed partial As(V) reduction to As(III) during scorodite transformation. These findings provide new insights into the stability and risk of scorodite under anaerobic conditions and help us understand the geochemical behavior of As in Fe-rich anaerobic environments.

CRediT authorship contribution statement

Jimei Zhou: Investigation, Methodology, Writing – original draft. **Yizhang Liu:** Investigation, Writing – review & editing. **Hongling Bu:** Writing – review & editing. **Peng Liu:** Methodology, Software, Review. **Jing Sun:** Writing – review & editing. **Fei Wu:** Investigation, Software. **Jian Hua:** Investigation. **Chengshuai Liu:** Conceptualization, Project

administration, Funding acquisition, Writing – review & editing.

Declaration of Competing Interest

The authors declare that they have no known competing financial interests or personal relationships that could have appeared to influence the work reported in this paper.

Acknowledgement

The research was supported by the National Natural Science Foundation of China (41921004, 42025705, and U1701241); the West Light Foundation and the Frontier Science Research Programme (QYZDB-SSW-DQC046) and Youth Innovation Promotion Association (2021399) of the Chinese Academy of Sciences; the Science and Technology Planning Project of Guangdong Province, China (2019GDSYL-0401003 and 2019GDASYL-0301002); the GDAS' Project of Science and Technology Development (2020GDASYL-20200102019). Synchrotron analyses were conducted at Sector 20-BM of Advanced Photon Source, Argonne National Laboratory.

Appendix A. Supporting information

Supplementary data associated with this article can be found in the online version at doi:10.1016/j.jhazmat.2022.128274.

References

AMCSD, American Mineralogist, Crystal Structure Database. ⟨http://rruff.geo.arizona.edu/AMS/amcsd.php⟩.
Amstaetter, K., Borch, T., Larese-Casanova, P., Kappler, A., 2010. Redox transformation of arsenic by Fe(II)-activated goethite (α-FeOOH). Environ. Sci. Technol. 44, 102–108.
Bluteau, M.C., Demopoulos, G.P., 2007. The incongruent dissolution of scorodite—solubility, kinetics and mechanism. Hydrometallurgy 87, 163–177.
Boland, D.D., Collins, R.N., Miller, C.J., Glover, C.J., Waite, T.D., 2014a. Effect of solution and solid-phase conditions on the Fe(II)-accelerated transformation of ferrihydrite to lepidocrocite and goethite. Environ. Sci. Technol. 48, 5477–5485.
Boland, D.D., Collins, R.N., Glover, C.J., Payne, T.E., Waite, T.D., 2014b. Reduction of U (VI) by Fe(II) during the Fe(II)-accelerated transformation of ferrihydrite. Environ. Sci. Technol. 48, 9086–9093.
Burton, E.D., Bush, R.T., Sullivan, L.A., Johnston, S.G., Hocking, R.K., 2008. Mobility of arsenic and selected metals during reflooding of iron- and organic-rich acid-sulfate soil. Chem. Geol. 253, 64–73.
Burton, E.D., Johnston, S.G., Watling, K., Bush, R.T., Keene, A.F., Sullivan, L.A., 2010. Arsenic effects and behavior in association with the Fe(II)-catalyzed transformation of Schwertmannite. Environ. Sci. Technol. 44, 2016–2021.
Burton, E.D., Bush, R.T., Johnston, S.G., Sullivan, L.A., Keene, A.F., 2011. Sulfur biogeochemical cycling and novel Fe-S mineralization pathways in a tidally re-flooded wetland. Geochim. Cosmochim. Acta 75, 3434–3451.
Catalano, J.G., Luo, Y., Otemuyiwa, B., 2011. Effect of aqueous Fe(II) on arsenate sorption on geothite and hematite. Environ. Sci. Technol. 45, 8826–8833.
Chai, L.Y., Yue, M.Q., Yang, J.Q., Wang, Q.W., Li, Q.Z., Liu, H., 2016. Formation of tooeleite and the role of direct removal of As(III) from high-arsenic acid wastewater. J. Hazard. Mater. 320, 620–627.
Cornell, R.M., Schwertmann, U., 2003. The Iron Oxides Structure, Properties, Reactions, Occurrences and Use, second ed. Wiley-VCH Verlag GmbH & Co. KGaA, Weinheim.
Cummings, D.E., Caccavo, J.F., Fendorf, S., Frank, R.R., 1999. Arsenic mobilization by the dissimilatory Fe(III)-reducing bacterium *Shewanella alga* BrY. Environ. Sci. Technol. 33, 723–729.
Drahota, P., Filippi, M., 2009. Secondary arsenic minerals in the environment: a review. Environ. Int. 35, 1243–1255.
Fan, C., Guo, C.L., Zeng, Y.F., Tu, Z.H., Ji, Y.P., Reinfelder, J.R., Chen, M.Q., Huang, W. L., Lu, G.L., Yi, X.Y., Dang, Z., 2019. The behavior of chromium and arsenic associated with redox transformation of schwertmannite in AMD environment. Chemosphere 222, 945–953.
Feng, Y., Liu, P., Wang, Y.X., Finfrock, Y.Z., Xie, X.J., Su, C.L., Liu, N., Yang, Y.Y., Xu, Y., 2020. Distribution and speciation of iron in Fe-modified biochars and its application in removal of As(V), As(III), Cr(VI), and Hg(II): an X-ray absorption study. J. Hazard. Mater. 384, 121342.
Ford, R.G., 2002. Rates of hydrous ferric oxide crystallization and the influence on coprecipitated arsenate. Environ. Sci. Technol. 36, 2459–2463.
Frierdich, A.J., Nebel, O., Beard, B.L., Johnson, C.M., 2019. Iron isotope exchange and fractionation between hematite (α-Fe_2O_3) and aqueous Fe(II): a combined three-isotope and reversal-approach to equilibrium study. Geochim. Cosmochim. Acta 245, 207–221.
Gallup, D.L., Mreiff, W., 1991. Characterization of geothermal scale deposits by Fe-57 mössbauer spectroscopy and complementary X-ray diffraction and infra-red studies. Geothermics 20, 207–224.
Handler, R.M., Frierdich, A.J., Johnson, C.M., Rosso, K.M., Beard, B.L., Wang, C.M., Latta, D.E., Neumann, A., Pasakarnis, T., Premaratne, W.A.P.J., 2014. Fe(II)-catalyzed recrystallization of geoethite revisited. Environ. Sci. Technol. 48, 11302–11311.
Hansel, C.M., Benner, S.G., Neiss, J., Dohnalkova, A., Kukkadapu, R.K., Fendorf, S., 2003. Secondary mineralization pathways induced by dissimilatory iron reduction of ferrihydrite under advective flow. Geochim. Cosmochim. Acta 67, 2977–2992.
Harvey, M.C., Schreiber, M.E., Donald, R.J., Griffith, M.M., 2006. Scorodite dissolution kinetics implication for arsenic release. Environ. Sci. Technol. 40, 6709–6714.
Hu, S.W., Lu, Y., Peng, L.F., Wang, P., Zhu, M.Q., Dohnalkova, A.C., Chen, H., Lin, Z., Dang, Z., Shi, Z.Q., 2018. Coupled kinetics of ferrihydrite transformation and As(V) sequestration under the effect of humic acids: a mechanistic and quantitative study. Environ. Sci. Technol. 52, 11632–11641.
Hu, S.W., Liang, Y.Z., Liu, T.X., Li, F.B., Lu, Y., Shi, Z.Q., 2020. Kinetics of As(V) and carbon sequestration during Fe(II)-induced transformation of ferrihydrite-As(V)-fulvic acid coprecipitates. Geochim. Cosmochim. Acta 272, 160–176.
Hua, J., Liu, C.S., Li, F.B., Zhu, Z.K., Wei, Z.Q., Chen, M.J., Gao, T., Qiu, G.H., 2019. Effects of rare earth elements' physicochemical properties on their stabilization during the $Fe(II)_{aq}$-induced phase transformation of ferrihydrite. ACS Earth Space Chem. 3, 895–904.
Hua, J., Fei, Y.H., Feng, C.H., Liu, C.S., Liang, S., Wang, S.-L., Wu, F., 2022. Anoxic oxidation of As(III) during Fe(II)-induced goethite recrystallization: evidence and importance of Fe(IV) intermediate. J. Hazard. Mater. 421, 126806.
Johnston, R.B., Singer, P.C., 2007. Solubility of symplesite (ferrous arsenate): implications for reduced groundwaters and other geochemical environments. Soil Sci. Soc. Am. J. 71, 101–107.
Johnston, S.G., Keene, A.F., Burton, E.D., Bush, R.T., Sullivan, L.A., 2011. Iron and arsenic cycling in intertidal surface sediments during wetland remediation. Environ. Sci. Technol. 45, 2179–2185.
Johnston, S.G., Burton, E.D., Keene, A.F., Planer-Friedrich, B., Voegelin, A., Blackford, M. G., Lumpkin, G.R., 2012. Arsenic mobilization and iron transformations during sulfidization of As(V)-bearing jarosite. Chem. Geol. 334, 9–24.
Johnston, S.G., Burton, E.D., Aaso, T., Tuckerman, G., 2014. Sulfur, iron and carbon cycling following hydrological restoration of acidic freshwater wetlands. Chem. Geol. 371, 9–26.
Karimian, N., Johnston, S.G., Burton, E.D., 2017. Antimony and arsenic behavior during Fe(II)-induced transformation of jarosite. Environ. Sci. Technol. 51, 4259–4268.
Ke, P.C., Song, K.Z., Ghahreman, A., Liu, Z.H., 2019. Improvement of scorodite stability by addition of crystalline polyferric sulfate. Hydrometallurgy 185, 162–172.
Kossoff, D., Welch, M.D., Hudson-Edwards, K.A., 2015. Scorodite precipitation in the presence of antimony. Chem. Geol. 406, 1–9.
Langmuir, D., Mahoney, J., Rowson, J., 2006. Solubility products of amorphous ferric arsenate and crystalline scorodite ($FeAsO_4{\cdot}2H_2O$) and their application to arsenic behavior in buried mine tailings. Geochim. Cosmochim. Acta 70, 2942–2956.
Liu, C.S., Zhu, Z.K., Li, F.B., Liu, T.X., Liao, C.Z., Lee, J.J., Shih, K., Tao, L., Wu, Y.D., 2016. Fe(II)-induced phase transformation of ferrihydrite: the inhibition effects and stabilization of divalent metal cations. Chem. Geol. 444, 110–119.
Liu, C.S., Massey, M.S., Latta, D.E., Xia, Y.F., Li, F.B., Gao, T., Hua, J., 2021. Fe(II)-induced transformation of iron minerals in soil ferromanganese nodules. Chem. Geol. 559, 119901.
Liu, P., Ptacek, C.J., Elena, K.M.A., Blowes, D.W., Gould, W.D., Finfrock, Y.Z., Wang, A. O., Landis, R.C., 2018. Evaluation of mercury stabilization mechanisms by sulfurized biochars determined using X-ray absorption spectroscopy. J. Hazard. Mater. 347, 114–122.
Liu, Y.N., Chen, M.J., Tong, H., Li, F.B., Liu, C.S., Hua, J., Long, S.Q., Gao, T., Liu, Y.H., Xia, Y.F., 2018. Oxidation mechanism of $Fe(II)_{aq}$-induced crystalline phase reconstruction of goethite couple with As(III). Acta Mineral. Sin. 39, 574–579.
Ma, X., Su, R., Zhao, X.M., Liu, S.J., Wu, X., Wang, S.F., Jia, Y.F., 2021. Phase transformation of hydrous ferric arsenate in the presence of Fe(II) under anaerobic conditions: implication for arsenic mobility and fate in natural and anthropogenic environments. Chem. Geol. 578, 120–321.
Maillot, F., Morin, G., Juillot, F., Bruneel, O., Casiot, C., Ona-Nguema, G., Wang, Y.H., Lebrun, S., Aubry, E., Vlaic, G., Brown, G.E., 2013. Structure and reactivity of As(III)- and As(V)-rich schwertmannites and amorphous ferric arsenate sulfate from the Carnoulès acid mine drainage, France: comparison with biotic and abiotic model compounds and implications for As remediation. Geochim. Cosmochim. Acta 104, 310–319.
Mandaliev, P.N., Mikutta, C., Barmettler, K., Kotsev, T., Kretzschmar, R., 2013. Arsenic species formed from arsenopyrite weathering along a contamination gradient in circumneutral river floodplain soils. Environ. Sci. Technol. 48, 208–217.
Manning, B.A., Fendorf, S.E., Goldberg, S., 1998. Surface structure and stability of arsenic(III) on goethite: spectroscopic evidence for inner-sphere complexes. Environ. Sci. Technol. 32, 2383–2388.
Mikutta, C., Mandaliev, P.N., Kretzschmar, R., 2013. New clues to the local atomic structure of short-range ordered ferric arsenate from extended X-ray absorption fine structure spectroscopy. Environ. Sci. Technol. 47, 3122–3131.
Mikutta, C., Schröder, C., Marc Michel, F., 2014. Total X-ray scattering, EXAFS, and Mössbauer spectroscopy analyses of amorphous ferric arsenate and amorphous ferric phosphate. Geochim. Cosmochim. Acta 140, 708–719.
Neumann, A., Olson, T.L., Scherer, M.M., 2013. Spectroscopic evidence for Fe(II)-Fe(III) electron transfer at caly mineral edge and basal sites. Environ. Sci. Technol. 47, 6969–6977.

Nordstrom, D.K., Alpers, C.N., Ptacek, C.J., Blowes, D.W., 2000. Negative pH and extremely acidic mine waters from Iron Mountain, California. Environ. Sci. Technol. 34, 254–258.

Paktunc, D., Bruggeman, K., 2010. Solubility of nanocrystalline scorodite and amorphous ferric arsenate: implications for stabilization of arsenic in mine wastes. Appl. Geochem. 25, 674–683.

Pedersen, H.D., Postma, D., Jakobsen, R., Larsen, O., 2005. Fast transformation of iron oxyhydroxides by the catalytic action of aqueous Fe(II). Geochim. Cosmochim. Acta 69, 3967–3977.

Perez, J.P.H., Tobler, D.J., Thomas, A.N., Freeman, H.M., Dideriksen, K., Radnik, J., Benning, L.G., 2019. Adsorption and reduction of arsenate during the Fe^{2+}-induced transformation of ferrihydrite. ACS Earth Space Chem. 3, 884–894.

Perez, J.P.H., Freeman, H.M., Brown, A.P., Genuchten, C.M.V., Benning, L.G., 2020. Direct visualization of arsenic binding on green rust sulfate. Environ. Sci. Technol. 54, 3297–3305.

Perl, J., Shin, J., Schümann, J., Faddegon, B., Paganetti, H., 2012. TOPAS: an innovative proton Monte Carlo platform for research and clinical applications. Med. Phys. 39 (11), 6818–6837.

Podgorski, J., Berg, M., 2020. Global threat of arsenic in groundwater. Science 368, 845–850.

Randall, S.R., Sherman, D.M., Ragnarsdottir, K.V., 2001. Sorption of As(V) on green rust ($Fe_4(II)Fe_2(III)(OH)_{12}SO_4{\cdot}3H_2O$) and lepidocrocite (γ-FeOOH): surface complexes from EXAFS spectroscopy. Geochim. Cosmochim. Acta 65, 1015–1023.

Ravel, B., Newville, M., 2005. Athena, artemis, hephasestus: data analysis for X-ray absorption spectroscopy using IFEFFIT. J. Synchrotron Radiat. 12, 537–541.

Revesz, E., Fortin, D., Paktunc, D., 2015. Reductive dissolution of scorodite in the presence of *Shewanella sp*. CN32 and *Shewanella sp*. ANA-3. Appl. Geochem. 63, 347–356.

Robins, R.G., 1987. Solubility and stability of scorodite $FeAsO_4{\cdot}2H_2O$: discussions and replies. Am. Mineral. 72, 842–844.

Smith, A.H., Lingas, E.O., Rahman, M., 2000. Contamination of drinking-water by arsenic in Bangladesh: a public health emergency. Bull. World Health Organ. 83, 177–186.

Sowers, T.D., Harrington, J.M., Polizzotto, M.L., Duckworth, O.W., 2017. Sorption of arsenic to biogenic iron (oxyhydr)oxides produced in circumneutral environments. Geochim. Cosmochim. Acta 198, 194–207.

Tian, Z.Y., Feng, Y., Guan, Y.Y., Shao, B.B., Zhang, Y.L., Wu, D.L., 2017. Opposite effects of dissolved oxygen on the removal of As(III) and As(V) by carbonate structural Fe (II). Sci. Rep. 7, 17015.

Wang, S.F., Lei, L., Zhang, D.N., Zhang, G.P., Cao, R., Wang, X., Lin, J.R., Jia, Y.F., 2020. Stabilization and transformation of selenium during the Fe(II)-induced transformation of Se(IV)-adsorbed ferrihydrite under anaerobic conditions. J. Hazard. Mater. 384, 121365.

Wang, S.L., Mulligan, C.N., 2008. Speciation and surface structure of inorganic arsenic in solid phases: a review. Environ. Int. 34, 867–879.

Wang, Y.H., Morin, G., Ona-Nguema, G., Juillot, F., Calas, G., Brown, G.E., 2011. Distinctive arsenic(V) trapping modes by magnetite nanoparticles induced by different sorption processes. Environ. Sci. Technol. 45, 7258–7266.

Yu, G.D., Fu, F.L., Ye, C.J., Tang, B., 2020. Behaviors and fate of adsorbed Cr(VI) during Fe(II)-induced transformation of ferrihydrite-humic acid co-precipitates. J. Hazard. Mater. 392, 122272.

Zhang, G.P., Yuan, Z.D., Lei, L., Lin, J.R., Wang, X., Wang, S.F., Jia, Y.F., 2019. Arsenic redistribution and transformation during Fe(II)-catalyzed recrystallization of As-adsorbed ferrihydrite under anaerobic conditions. Chem. Geol. 525, 380–389.

Zhang, W.F., Lu, H.B., Liu, F., Wang, C.L., Zhang, Z.H., Zhang, J., 2021. Hydrothermal treatment of arsenic sulfide slag to immobilize arsenic into scorodite and recycle sulfur. J. Hazard. Mater. 406, 124735.

Zhou, J.M., Shu, Chen, Jing, Liu, Frost, R.L., 2018. Adsorption kinetic and species variation of arsenic for As(V) removal by biologically mackinawite (FeS). Chem. Eng. J. 354, 237–244.